Construction and Building Materials 352 (2022) 128965

Contents lists available at ScienceDirect

Construction and Building Materials

journal homepage: www.elsevier.com/locate/conbuildmat

Calibration of a total strain crack model for adobe masonry based on compression and diagonal compression tests

J.M. Fages [a], N. Tarque [b,c], J.D. Rodríguez-Mariscal [a], M. Solís [a,*]

[a] Escuela Técnica Superior de Ingeniería, Universidad de Sevilla, Camino de los Descubrimientos s/n, 41092 Sevilla, Spain
[b] Department of Continuum Mechanics and Structures, Universidad Politécnica de Madrid, C/ Prof. Aranguren 3, 28040, Madrid, Spain
[c] GERDIS Research Group, Civil Engineering Division, Pontificia Universidad Católica del Perú, Av. Universitaria, 1801, Lima, Peru

ARTICLE INFO

Keywords:
Adobe masonry
Numerical simulation
Total strain crack model
Experimental calibration

ABSTRACT

Although it has good compressive behavior, adobe masonry is classified as a quasi-brittle material mainly due to its relative low tensile strength and softening behavior after the peak tensile strength. The behavior, plus the high variability in the adobe mechanical properties, makes it difficult to evaluate the performance of entire adobe buildings. For such a purpose, the development of reliable and computationally efficient numerical approaches is required. This work shows a numerical methodology to calibrate the main mechanical parameters to be used in the numerical modeling of adobe samples following the finite element method (FEM) by using the Total-Strain Crack model. The present paper shows that this numerical model is able to represent the nonlinear behavior of the adobe masonry. The calibration process is based on preliminary experimental tests performed on masonry prisms (piles and wallets) subjected to axial compressive and diagonal compression loads, respectively. The main results show that it is possible to model adobe masonry in practice. A consistent reproduction of the cracking pattern from experimental tests is obtained. By using the calibrated properties, this work may be extended to evaluate the seismic vulnerability of complete adobe structures.

1. Introduction

Earth is one of the most elementary and widely used building material along history and all around the world. Its extensive use persists today only in low-income areas where its low-cost and availability make it the best choice for domestic dwelling [1]. In high-income rates areas of the world, earth has been progressively substituted by more resistant and structurally efficient materials, mainly reinforced concrete, steel and confined masonry using fired clay or concrete bricks. However, from a historical perspective, this phenomenon has been a very recent and fast change. In these regions, traditional knowledge about earthen construction has almost been lost within just a couple of generations. As a consequence of this rapid change as part of the current modern technological development period, earthen construction fell outside the interest of the global technical and scientific community. As a result, no modern and rigorous codes of practice nor standards have been developed for this material [2–4].

However, as a matter of fact, on the one hand, earth is still being used as the main building material for a high portion of world population and, on the other hand, there is a vast amount of earthen cultural heritage to be conserved in areas where earth is not any more a commonly used building material [5,6]. Moreover, in high-income countries, where concern about the environmental impact of the construction activity is gaining relevance, the use of natural and environmentally friendly materials is attracting attention of politics, technicians and society [7,8]. For these reasons, the scientific study of earth as building material is necessary to provide a safe and reliable framework for its use and conservation.

Among the different traditional building techniques based on the use of raw earth, adobe masonry is one of the most well-known and widespread around the world. Adobe bricks are made from a mixture of soil, water and vegetable fibers. The adobe masonry walls are built by using fresh mud mortar to glue the adobe bricks. As a result, because of the use of similar material for the bricks and for the mortar, adobe masonry may be considered a uniform and homogeneous material, in contrast with other types of masonry that use materials with different properties for the bricks (stone, concrete, fired clay bricks) and for the mortar (modern cement-based or traditional lime-based mortars). Thus, the assumption of a homogeneous macro-model behavior for adobe masonry is a practical and reasonable approach [9,10], specially when dealing with large size structures.

* Corresponding author.
E-mail address: msolis@us.es (M. Solís).

https://doi.org/10.1016/j.conbuildmat.2022.128965
Received 31 March 2022; Received in revised form 21 August 2022; Accepted 22 August 2022
Available online 12 September 2022

Adobe masonry is mainly used in small to medium size buildings. A vast amount of examples and construction types can be found around the 5 continents. In Spain, adobe has been extensively used for rural houses until the middle of the 20th century [11–13]. Nowadays, many adobe houses still exist in many villages, though most of the population (even in those villages and specially the youngest people) are not aware of the existence of this building material. Thus, repair and conservation of these constructions is difficult to be properly and safely addressed without specific and reliable technical knowledge.

Modern scientific research about adobe masonry is mainly dedicated to the experimental mechanical characterization of adobe bricks and masonry [14,15]. Proposals for the use of natural and synthetic reinforcements to enhance the mechanical performance of the masonry have also been experimentally explored. The experimental analysis has mainly consisted of compression, shear and diagonal compression tests of adobe walls. From these tests, mechanical properties such as compressive strength, compressive and shear stiffness, and tensile strength can be estimated. Unfortunately, most of the experimental research works have addressed specific tests of specimens built with specific adobes. As a result, and because of the scattering of the estimated values for the different properties for different adobe types, a complete mechanical model based on experimental results cannot be developed for any of the tested masonries.

As for any building material, besides the required experimental knowledge to estimate expected values of the mechanical properties, it is necessary to develop numerical models that can be eventually used in practice for the structural design of new constructions, as well as to predict the response and design strategies for the conservation of existing constructions. However, there is little literature regarding the numerical modeling applied to adobe masonry [14–21], in comparison not only to other common building materials such as reinforced concrete, but also to other traditional ones such as stone masonry, for instance. One of the reasons for the little work developed up to now is the lack of reliable reference data of material properties for modeling adobe in the inelastic range.

Although the mud mortar and the adobe bricks are frequently made from the same soil, the bricks' geometrical arrangement makes the composite anisotropic. Then, the assumption of having an isotropic and homogeneous material simplifies studying the composite's numerical structural behavior. Like many other quasi-brittle materials, the adobe masonry may have a different modulus of elasticity in its three perpendicular directions. However, in this work, the adobe masonry is assumed to be homogeneous and isotropic, with the same Young modulus in tension and compression [16,19,21]. This is a clearly a limitation of the proposed numerical approach. Still, after calibrating the mechanical parameters and proposing one single constitutive law (compression–tension), the numerical predictions can be useful in practice for the analysis of stress and strain fields and cracking patterns [22].

According to [21], the numerical modeling of adobe structures can be done with the Finite Element Method (FEM), the Distinct Element Method (DEM) or the equivalent frame model. Within the FEM, there exist three approaches for modeling unreinforced masonry in general [23]: detailed numerical modeling, simplified numerical modeling, and macro modeling. In all of them, it is important to calibrate properly the material properties of each masonry component, with special attention to the non-linear part of the constitutive laws. This is a critical issue for the adobe material, since it breaks suddenly and the inelastic behavior, especially in tension, controls the crack propagation and stress re-distribution. Examples of modeling adobe masonry following the simplified micro-modeling approach can be found in [16–18]. Applications of the macro-modeling have been developed in [9,10,19]. In all these previous works, the modeling was limited to small adobe walls or adobe structures tested in structural laboratories, for which limited experimental data was available.

In this paper, experimental data for compression tests, diagonal compression tests and splitting tests of the same adobe masonry are used to build a numerical model for the simulation of the experimental tests of adobe masonry walls. From these tests, reference experimental values for the compressive constitutive law and tensile strength are used to build a total strain crack model for the adobe masonry. The experimental results from the diagonal compression tests are used as a reference benchmark problem to validate the numerical results. The performance of the total strain crack model using a rotating crack approach to consider the presence of damage is investigated. The paper analyzes the capability of the proposed model to simulate the behavior of the tested specimens. It includes a sensitivity analysis of the different parameters involved in the definition of the numerical model, specially those related with fracture mechanics and plasticity for which no experimental information is available. The outline of the paper is as follows. First, the experimental tests and reference data are presented. Next, some relevant theoretical aspects about the numerical modeling are reviewed. Then, the paper presents the details about the numerical modeling strategy and the main results, including the sensitivity analysis of constitutive model parameters and the proposal for specific values based on the agreement with the experimental results and reference values from previous research works. Finally, conclusions are drawn and future research objectives are outlined.

This work allows researchers and practitioners to perform further numerical modeling of adobe structures by using the calibrated material properties reported here, especially for adobe constructions made with soils from the Guadalquivir river bank in Sevilla. The results – in terms of good agreement between the numerical calibration and experimental data – validate the macro modeling approach for the analysis of complete adobe masonry structures, as also supported by other researchers.

2. Experimental tests and data results

The available experimental load–strain curves used for the development and analysis of the numerical models come from simple compression and diagonal compression tests on adobe walls. These walls were built using traditional techniques in the Structures Laboratory from University of Sevilla in Spain. For the adobe brick production, a portion of fresh mixture was manually thrown into a mold with the desired dimensions for the bricks. Once the mold was filled with fresh mixture, it was removed and the resulting fresh brick was dried under ambient conditions (warm and dry conditions are preferred but protected from direct sunlight to avoid cracking due to a too rapid drying process). Once the bricks were dried after 28 days, adobe walls were built using fresh mud mortar for the masonry joints (20 mm thickness). In this work, the dimensions of the bricks were $80 \times 160 \times 320 mm^3$ (Fig. 1). The soil was collected from the riverbank of Guadalquivir River in Seville (Spain). The soil composition (in weight) was 60% of sand, 20% of silty soil and 20% of clay soil. The Liquid Limit and Plastic Limit of the soil were 23.1 and 17.2, respectively. Wheat straw was added to the fresh mud during the manufacturing process (1% in weight). The length of the straw fibers was 50 mm approximately. Moisture content (in weight) during the manufacturing process was 1.3%.

2.1. Axial compression tests

Nine adobe masonry walls were built and tested in compression. Each wall was made of 6 adobe rows of 1 and half brick width, making an overall dimension of 580 mm height and 500 mm width approximately. A monotonically increasing compressive load was applied until failure at 1 mm/min displacement controlled rate. Vertical strains were measured through 2 LVDT displacement sensors fixed at each side of the walls. Each of these sensors measured the relative displacement between two points located 200 mm apart as shown in Fig. 2(a). The typical failure pattern was vertical fissures and X-shape cracking in all

(a) (b)

Fig. 1. Adobe bricks: (a) molded and air dried and (b) stored in laboratory conditions (temperature between 15 and 25 °C and humidity around 50%.).

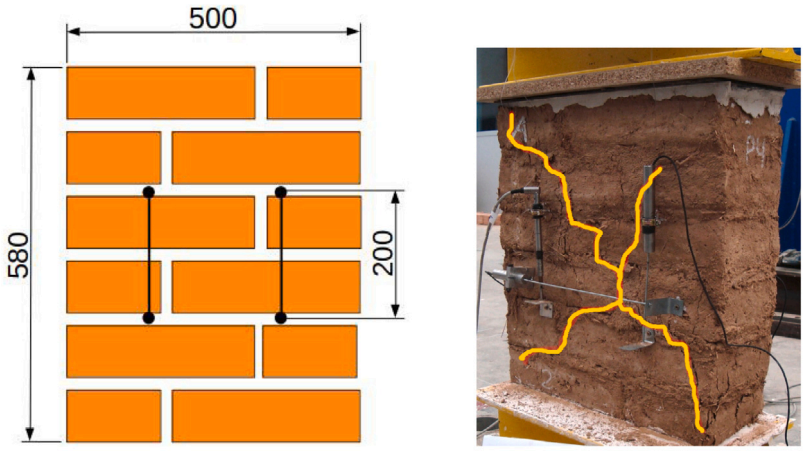

(a) (b)

Fig. 2. (Compression test: (a) Scheme of the walls tested including the displacement sensors location (units in mm) and (b) Experimental set-up and illustration of the failure pattern.

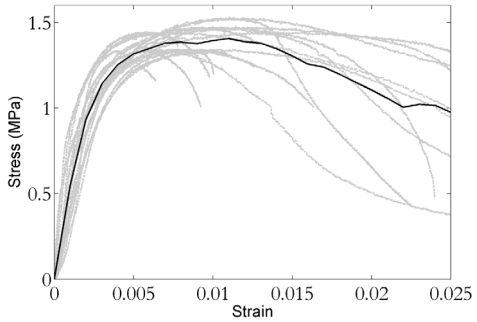

Fig. 3. Average experimental compressive constitutive law (solid dark line) and experimental curves obtained from all tests (dashed gray lines).

of them, those relative to the Poisson effect (Fig. 2(b)). The stress–strain relationship in compression for the adobe masonry is obtained from the average experimental values collected from all the walls and vertical sensors. Fig. 3 shows the average stress–strain curve along with the experimental stress–strain curves. The compressive strength defined from this curve is 1.39 MPa. Further details about the experimental characterization of the compressive behavior of the adobe masonry can be found in [24].

2.2. Diagonal compression tests

For the diagonal compression tests, the adobe masonry wall specimens were manufactured by following the design specifications from the ASTM standard [25]. The nominal dimensions were 900 × 900 × 160mm^3, which consist of 9 rows of bricks with 2.5 bricks per row. A total of 8 walls were built and tested following ASTM and RILEM standards for masonry walls [25,26]. Fig. 4 illustrates the experimental set-up. Four LVDT displacement sensors were located at each side of the wall to measure the relative displacements (macrostrains) in the horizontal and vertical directions, as shown in Fig. 4. The range of observed experimental strains and their average value will be considered as a reference for comparison purposes with the numerical model predictions. Fig. 5 shows the average stress–strain curve along with the experimental stress–strain curves. Further details about these experimental tests are included in [20].

2.3. Analysis of reference experimental data in the literature

The use of different soils, dimensions for the bricks, mortar properties, dimensions of masonry specimens, manufacturing process, etc. in different research works, leads to different values of mechanical properties for adobe masonry. However, despite the scattering of the experimental values of compressive, shear and tensile strength and stress–strain relationships, a limited practical range for these properties can be estimated from available data in the literature. An interesting and comprehensive review of results from different experimental works can be found in [14].

Regarding the behavior in compression of the adobe masonry, values of compressive strength are found between 0.33MPa [27] and 3.28 MPa [28]. However, in the first case, adobe walls were built by reusing adobe blocks from ancient demolished constructions. In the latter, a special mortar with gravel was used to joint the adobe blocks. For usual new adobe walls, the compressive strength is more likely to be within the range of 1–2 MPa, as it is the case for the

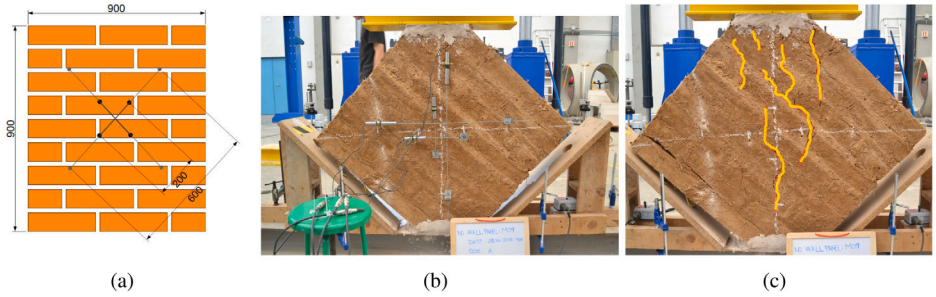

Fig. 4. Diagonal compression test: (a) scheme of the wall including the displacement sensors positions (units in mm), (b) Experimental set-up and (c) Illustration of the experimental crack pattern.

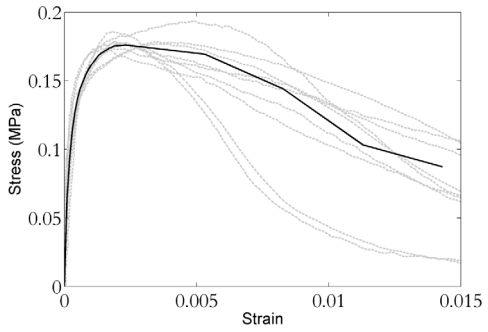

Fig. 5. Average experimental diagonal compressive constitutive law (solid dark line) and experimental curves obtained from all tests (dashed gray lines).

Table 1
Resume of the experimental results of the laboratory tests (in MPa).

Axial compression tests		Diagonal compression tests		Splitting tests
f_c	E	f_t	G	f_t
1.39	642[a]	0.18	782[b]	0.17[c]

[a]Secant modulus at 1/3 of the compressive strength.
[b]Secant modulus at 1/3 of the shear strength.
[c]Indirect tensile strength.

reference experimental data used here (1.39 MPa) (Table 1) and some others (0.94 MPa in [29], 1.73 in [30], 2.02 in [31]). For the estimation of compressive stiffness, the results are also affected by the methodology used for the evaluation of the Young modulus. However, when considering a common procedure for the estimation, a practical range for the estimation of the Young modulus can be identified. For the secant modulus at 1/3 of the compressive strength, a value of 757 MPa is found in [27], 803 MPa in [17] and 783–899 in [31]. These values are in good agreement with the value of 642 MPa obtained for the reference experimental tests in the present work, Table 1. For the peak strain, consistent values were obtained in [17] (0.55), [31] (0.45) and the present work (0.84).

From the diagonal compression tests, a shear strength value of 0.21 MPa and a shear modulus at 1/3 of the shear strength of 397 MPa was obtained in [17]. In [27], a much smaller value of the shear strength was obtained (0.03 MPa), but ancient adobe bricks were used for building the masonry walls. However, a similar value of the shear modulus was obtained (413 MPa). In the reference experimental tests considered in this paper, the obtained shear strength was 0.18 MPa and the shear modulus was found to be 268 MPa for the chord modulus between 1/3 and 2/3 of the shear strength and 782 MPa for the secant modulus at 1/3 of the shear strength, Table 1.

3. Numerical macromechanical models for adobe masonry

The numerical analysis of masonry structures can be performed using different methods such as limit analysis, the finite element method and the discrete element method. Another approach consists of idealizing the structure through an equivalent frame where each wall is discretized by a set of masonry panels (piers and spandrels) [21,32]; here the non-linear response is placed with plastic hinges at the element ends. However, to the authors' knowledge, no specific applications of this approach have been specifically developed yet for adobe masonry. They exist just for fire clay brick and stone masonry. For the numerical modeling of walls, one of the main difficulties is the simulation of brittle materials: bricks and mortar. These materials have a non-linear behavior due to their little or almost zero tensile capacity. In compression, they can easily resist gravity loads in the elastic range.

There are two principal numerical modeling strategies for masonry walls. They are the micro-modeling and the macro-modeling approach. The micro-modeling consists of discretizing in detail the components of the masonry walls, taking into account bricks and mortar separately. [23,33] distinguish between detailed and simplified micro-modeling within this micromechanical approach. The difference between these two is that in the simplified micro-modeling (also called meso-modeling), the bricks are continuous elements and the mortar joints are discontinuous. In contrast, both mortar and brick are continuous elements in the detailed micro-modeling, and the brick–mortar interfaces are discontinuous elements.

The macro-modeling represents bricks and mortar by a single equivalent and homogeneous material. It is assumed that the entire wall is made up of a single continuous material without differentiating the limits of the masonry components and considering the damage smeared into the continuum. The macro-modeling is commonly used to analyze large structures due to its lower calculation demands. Also, it is applicable when the structure is composed of solid walls with sufficiently large dimensions where the stresses across or along a macro-length are essentially uniform [23]. The input material properties are established by homogenization, which relates average masonry strains and average masonry stresses [16,34]. The homogenization involves the simplification of the composite brick–mortar into one equivalent material; this means creating a new material, which represents the behavior of the masonry. A different homogenization can be performed in the direction parallel and perpendicular to the bed joints to consider the different behavior along both directions [35]. This technique has been used to analyze arch bridges, historical buildings, mosques and cathedrals [34] based on tension–compression damage finite element formulation. However, this technique generally introduces a limitation, which is to assume a homogeneous and isotropic material, as in the case of adobe structures. To have a better representation of the non-isotropy of the masonry, different homogenization techniques can be found in the literature, especially for reproducing the in-plane and out-of-plane actions [36–40].

Another type of simplified numerical modeling is the equivalent frame model. It uses linear beam–column elements for representing the

masonry walls. Despite considering linear elements, the non-linearity of the wall (in tension, bending and shear) can be represented by inserting plastic hinges inside each beam–column element.

In this work, the macro-modeling approach was used for modeling the described experimental tests, following a parametric calibration of the constitutive laws for the application of a total-strain crack model implemented in Midas FEA software.

3.1. The total-strain crack model

The total-strain crack model uses the macro-modeling approach for masonry structures considering a non-linear isotropic-homogeneous material. The total-strain crack model was originally introduced for reproducing the cracking and stress distribution in concrete under a non-linear behavior [41,42]. It uses the macro-modeling approach considering a non-linear isotropic-homogeneous material. This model establishes a criterion for crack formation and growth for quasi-brittle materials. This criterion is based on the softening that occurs once the material's tensile strength is exceeded, being this softening dependent on the opening of the crack. The material behavior in the total-strain crack model is defined by a tension and compression constitutive law (stress–strain relationships). Although it was originally developed for concrete, it is used in this work for reproducing the non-linear behavior of adobe masonry. A comprehensive work, where many numerical validations of in-plane and out-of-plane experimental tests of masonry composites can be found in [43]. Also, new developments of the total-strain crack model but considering the orthotropic masonry characteristics have recently been performed by [44], concluding that although constitutive models for masonry have progressed in the recent years, they still need to be improved.

The total-strain crack model does not divide the total strain into strain components, making the analysis more accessible and faster in FEM programs. The advantage of using this model is the easy formulation of the algorithm since it only uses stress–strain relationships. In this model, the stress is assumed to be function of the total strain [45].

When the material is cracked, it ceases to have isotropic properties, becoming an anisotropic material, calculating the normal stresses and tangential stresses on the crack surface. By considering just perpendicular crack angles, the total-strain crack model can be classified into an orthogonal crack model. The shape of the tensile-softening diagram and the material fracture energy mainly controls the crack propagation. The fracture energy is related to the area under the inelastic part of the stress vs strain curve. It can also be expressed in the stress vs displacement curve, where the displacement is computed as the strain times the element characteristic length h. This length is the diagonal of a 4-node quadrilateral linear shell element, or the half of the diagonal of a 8-node quadratic shell element [16]. Furthermore, a mesh sensitivity analysis should be done to analyze the maximum mesh size to be used without altering the stress–strain results. This is done by analyzing a masonry sample with different mesh sizes. The final mesh size may be taken as the larger one having same stress–strain results as smaller mesh sizes.

The evaluation of the crack state of the element takes place at its integration points, and it is not possible to determine the exact position of the crack within the element. Depending on the shear stress–strain relationship, two approaches can be considered for smeared cracking modeling:

(a) Fixed-crack model (Fig. 6(a)): The crack direction does not change once the cracks are formed. Therefore, after the crack's directions are fixed, normal and tangential stresses appear. In this model, the shear stiffness reduction of the material because of cracking is defined by a factor affecting the shear modulus (ranging from 0 to 1).

(b) Rotating-crack model (Fig. 6(b)): in this case, the orientation of the crack, and therefore of the directions of principal stresses, can be reoriented for each load step. As a result, they align accordingly with the different stress and strain fields through the loading process. As a consequence, tangential stresses do not appear.

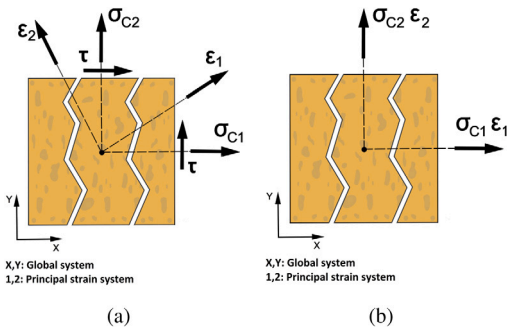

Fig. 6. Scheme of stress at crack surfaces for (a) fixed crack and (b) rotating crack model.

In both fixed and rotating crack models, the crack initiates in the directions of the principal strains. In addition, due to lateral confinement effects, the compressive stress–strain relationship can be modified to incorporate the effects of increased isotropic stress. When the material is cracked, lateral tensile strains perpendicular to the principal compressive direction reduce the compressive strength. The concept of failure function is introduced to compute the compressive stress, which causes failure as a function of the confining stress in the lateral directions. If the material is cracked in the lateral directions, the peak compressive stress and the strain at peak compressive stress are reduced by factors proposed by [46].

3.2. Constitutive laws

As aforementioned, the compression and tension constitutive laws are the main ingredients for numerical modeling using the total-strain crack model. The definition of the isotropic behavior is defined through a constant Poisson modulus. In addition, for the fixed-crack model, the shear stiffness at cracked elements is reduced by a factor between 0 and 1.

In this research, the experimental compression tests allowed the definition of a parabolic compressive stress–strain curve, assuming a hardening–softening behavior represented by a fracture energy. The diagonal compression tests provided an experimental estimate of tensile strength, which can be used for the definition of a linear tensile constitutive law followed by an exponential softening law [47], where the fracture energy is related to the equivalent length or crack bandwidth of the elements (parameter h). Apart from the fracture energy and tensile strength, the stiffness of the initial linear behavior has to be defined.

4. Numerical modeling strategy

The numerical model was built using Midas FEA software. A 2D model was built assuming a plane stress state. 8 node quadrilateral and 6 node triangular quadratic shell elements were used when necessary to adapt the mesh for geometric transitions. A plane stress is suitable to represent the experimental tests since only in-plane loads are considered and there is no out-of-plane response. The out-of-plane deformations due to Poisson's effect are implicitly considered in the plane stress assumption. However, the connection between the headings and the masonry produces a physical local 3D confinement effect at those zones that is not properly considered in a plane stress model. Thus, the numerical stresses and strains close to those areas are considered to be not realistic and are excluded from the analysis.

The vertical displacements at the bottom face of the walls were fixed, whereas uniform values were subsequently imposed at the top face, simulating the experimental displacement controlled configuration. Regarding the horizontal displacements at these boundaries, 1D

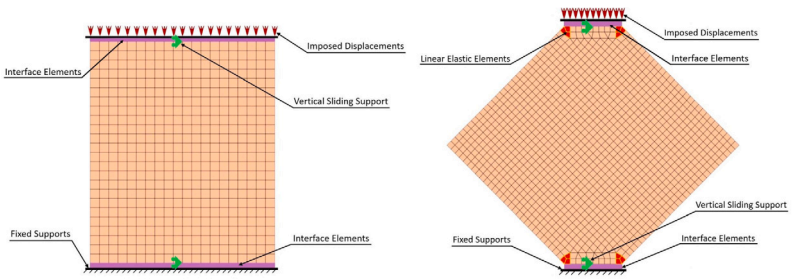

Fig. 7. Finite element mesh, boundary conditions and transition elements used for (a) simple compression and (b) diagonal compression simulations.

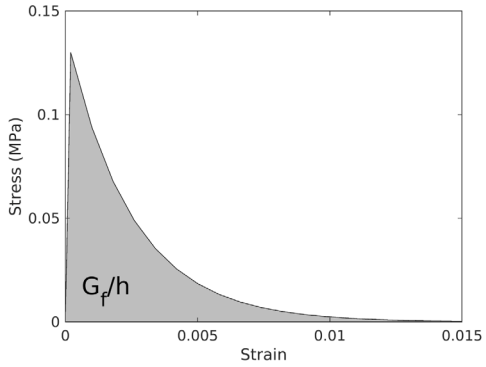

Fig. 8. Tensile constitutive law for tensile strength of 0.13 MPa, initial elastic modulus of 642 MPa, fracture energy of 0.008 N/mm and element characteristic length of 25 mm.

interface elements were introduced with a horizontal friction coefficient of 0.3. These interface elements introduce a trade-off between totally restrained or unconfined situations if the horizontal displacements are restrained or free at the bottom and top faces of the walls, respectively. 40 and 25 interface elements were used for the simulation of the compression and diagonal compression tests, respectively. Moreover, in order to avoid unrealistic local failure mechanisms at the areas close to those boundaries, a linear elastic behavior was assumed for irregular elements localized at those areas (see Fig. 7). Fig. 7 shows pictures of the mesh used for the simple compression and diagonal compression simulations, including a schematic representation of the imposed boundary conditions and the aforementioned interface and linear elastic elements.

According to the values of the maximum experimentally imposed displacements, a maximum vertical displacement of 20 mm and 10 mm is imposed at top sides of the walls for the compression and diagonal compression tests simulations, respectively, divided into 20 uniform load steps for which the solution is found. The evolution of the different magnitudes during the loading process is obtained from the set of results obtained for all load steps.

4.1 Constitutive model

4.2 Compressive constitutive law

The average stress–strain law obtained from the compressive tests (Fig. 3) is used to define the compressive constitutive law. Their values are introduced through a set of stress–strain values.

4.3 Tensile constitutive law and fracture energy

The tensile constitutive law and fracture energy are critical parameters for which unfortunately there is little reference experimental data in the literature. In this study, reference values of the tensile strength obtained by the authors in a previous work have been considered [20], whereas a reference model constitutive model for quasi-brittle materials is adopted, using some exploratory reference values for the tensile fracture energy considered by other authors.

The tensile constitutive law is defined by assuming an initial linear elastic behavior until the tensile strength is reached, followed by an exponential softening law due to damage. The area below this stress–strain curve is the fracture energy (G_f). This type of constitutive model is usually considered for quasi-brittle materials. However, when softening occurs, the governing differential equations lose ellipticity (tangent modulus is no longer positive), and the boundary value problem describing the structural response becomes ill-posed, which means to have a non-unique solution of the problem. This phenomenon was deeply analyzed in [48–51]. To solve this issue, it is suggested to specify the tensile softening but localized into a size band h, which is the characteristic element length related to the mesh dimension [48]. In this case, the stress–strain curve is no longer considered as a unique curve characterizing the material but converted into a stress–displacement curve. Since the dissipated energy per unit area has to be equal to the fracture energy G_f (a material property), a new parameter $g_f = G_f/h$ is derived to guarantee equality [48,49]. The units of g_f are N/mm. This procedure is known as the crack band approach or fracture energy approach, and helps to solve the strain localization problem and alleviate mesh dependency [51]. Fig. 8 illustrates the constitutive tensile law for tensile strength of 0.13 MPa, initial elastic modulus of 642 MPa, a fracture energy of 0.008 N/mm and element characteristic length of 35.35 mm (corresponding to the diagonal length of a square element of 25 mm side length).

The tensile behavior plays a critical role in the behavior of the material since it controls its fracture behavior and therefore the failure mechanisms of the specimen, redistribution of stresses and strains, etc. Unfortunately, there is major uncertainty for its definition based on experimental results, because of the difficulty in obtaining reliable values for the tensile strength and fracture energy.

Regarding the tensile strength, a value of 0.17 MPa was obtained by the authors from splitting tests of cylindrical samples of the same material as the adobe brick [20]. From the diagonal compression tests presented in the same work [20], different values of the tensile strength were estimated assuming a pure shear stress state and the elastic solution of this kind of test. Values of 0.181 MPa and 0.13 MPa were obtained from both assumptions, respectively.

For the first elastic range, a reference value can be also obtained from the initial Young modulus of the experimental compressive constitutive law. The secant value of the Young modulus estimated in [24] at 1/3 of the compressive strength is used as a reference value in this study (642 MPa).

The fracture energy is a critical parameter for which the experimental determination is complex and there are very few and scatter reference experimental values in the literature. In the work of Almeida [52], they found a tensile fracture energy of 0.0045 N/mm and 0.015 from direct tensile tests on notched samples of sandwich adobe specimens (with mud mortar at interfaces) and simple notched simple specimens respectively. An intermediate value (0.007 N/mm) was obtained in [53] from direct tensile tests of sandwich specimens of adobe for which a tensile strength of 0.15 MPa was estimated from splitting tests. In previous numerical approaches for the simulation of adobe masonry, a value of 0.01 N/mm was considered in [16] for

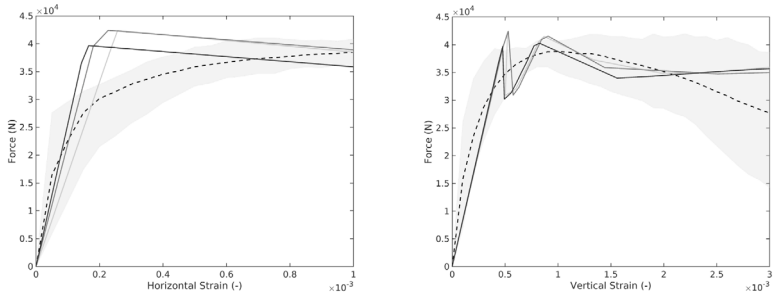

Fig. 9. Relationship between applied force and (a) horizontal and (b) vertical strains in the diagonal compression test simulation for tensile Young modulus $E_{0-1/3}$ = 642 MPa (dark gray line), $E_{0-2/3}$ = 533 MPa (medium gray line) and $E_{1/3-2/3}$ = 497 MPa (light gray line). The shaded area represents the envelope of the experimental results. The dashed line represents the average experimental stress–strain curve.

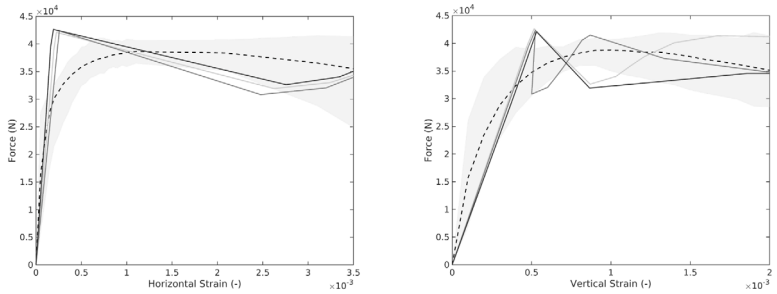

Fig. 10. Relationship between applied force and horizontal strains in the diagonal compression test simulation for Poisson modulus ν = 0.3 (dark gray line), ν = 0.11 (medium gray line) and ν = 0.05 (light gray line). The shaded area represents the envelope of the experimental results.

the analysis of the shear behavior of adobe walls. For the case of rammed earth, Miccoli et al. [28] used a value of 0.029 times the tensile strength, as recommended for historical masonry. Based on these reference values, a range between 0.004 and 0.02 will be considered in the present study.

4.4 Poisson modulus

Few experimental studies have addressed the experimental determination of the Poisson ratio for adobe masonry yet. The determination of small transversal strains that are much influenced by the progressive cracking is experimentally difficult to achieve. Thus, the experimental estimates are uncertain and the scattering of the obtained results is very significant. Different studies have obtained values from 0.05 to 0.5 [14], although most of them point to a range between 0.05 and 0.3. Thus, this range is considered as a reference to be considered in the present work. It has also been observed an increasing trend of the value of the Poisson modulus as the stress level increases [24,29], but this phenomenon cannot be introduced in the present numerical approach.

5. Sensitivity analysis of constitutive model parameters

In this section, the influence of the tensile Young modulus, Poisson modulus, tensile fracture energy, tensile strength and element size are analyzed independently. A selection of a suitable value for each parameter is performed by comparing the experimental and numerical results. For such a purpose, the relationship between the applied force and the horizontal strains in the diagonal compression is considered, since it is the most sensitive experimental feature from those available. For the most critical parameters, vertical strains are also analyzed. In the numerical model, since the boundary conditions are defined in terms of imposed displacements, the applied force is evaluated from the reaction forces. For a consistent comparative analysis, the strains from the numerical model are obtained from the relative displacements between nodes located at the same positions where the displacement transducers were fixed to the wall in the experimental tests.

Table 2
Parameters for sensitivity analysis of constitutive model.

Parameter	Range	Reference fixed value
Tensile Young modulus	460–642 MPa	642 MPa
Poisson modulus	0.05–0.3	0.3
Tensile fracture energy	0.004–0.02 N/mm	0.008 N/mm
Tensile strength	0.12–0.17 MPa	0.13 MPa
Element size	25–50 mm	25 mm

The sensitivity analysis is performed by studying the influence on the numerical results of each single parameter within a certain range, considering a reference fixed value for the rest of the parameters as defined in Table 2.

5.1. Tensile Young modulus

Fig. 9 shows the results obtained for the three different estimates of the Young modulus obtained from the compressive tests of adobe wallets [24]. They correspond to the secant modulus at 1/3 and 2/3 of the compressive strength ($E_{0-1/3}$ = 642 MPa and $E_{0-2/3}$ = 533 MPa, respectively) and the tangent modulus between 1/3 and 2/3 of the compressive strength ($E_{1/3-2/3}$ = 497 MPa). The results show that the estimate that better fits the initial compressive stiffness ($E_{0-1/3}$) provides a better fit with the experimental results from diagonal compression tests. This can be observed in Fig. 9(a) for the vertical stiffness. It is clear how the tensile stiffness affects mainly the vertical stiffness at lower load levels. In contrast, the horizontal strains are barely affected by the value of the Young modulus (Fig. 9(b)) at the initial stage. The tensile Young modulus also affects the strength of the wall, since (for the same tensile strength and fracture energy) a lower tensile stiffness increases ductility and delays the specimen failure.

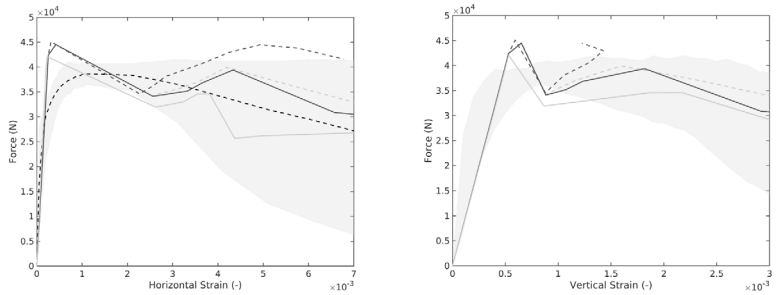

Fig. 11. Relationship between applied force and (a) horizontal strains and (b) vertical strains in the diagonal compression test simulation for a fracture energy value of 0.004 N/mm (solid dark gray line), 0.008 N/mm (solid light gray line), 0.01 N/mm (dashed dark gray line) and 0.02 N/mm (dashed light gray line). The shaded area represents the envelope of the experimental results.

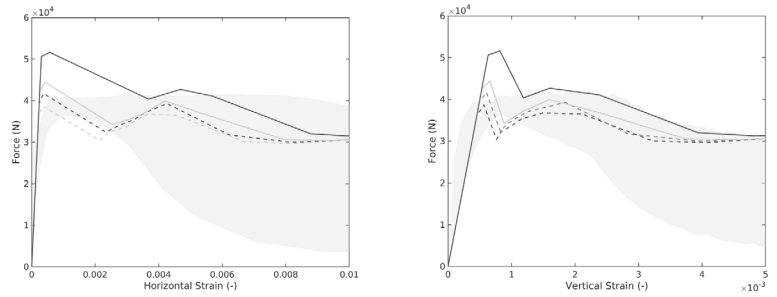

Fig. 12. Relationship between applied force and (a) horizontal strains and (b) vertical strains in the diagonal compression test simulation for a tensile strength of 0.17 MPa (solid dark gray line), 0.14 MPa (solid light gray line), 0.13 MPa (dashed dark gray line) and 0.12 MPa (dashed light gray line). The shaded area represents the envelope of the experimental results.

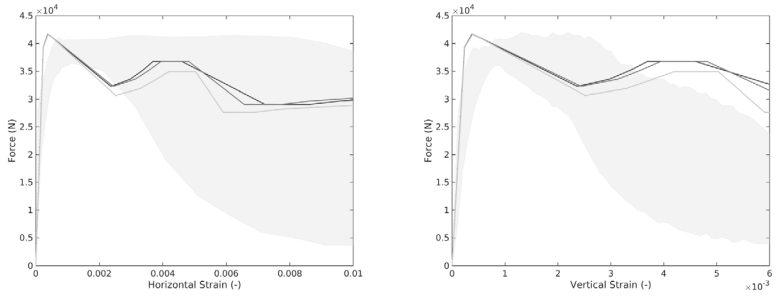

Fig. 13. Relationship between applied force and (a) horizontal strains and (b) vertical strains in the diagonal compression test simulation using an element size of 25 mm (dark gray line), 35 mm (medium gray line) and 50 mm (light gray line). The shaded area represents the envelope of the experimental results.

5.2. Poisson modulus

Fig. 10 shows that the Poisson modulus has little influence on the values of the horizontal strains whereas it affects the numerical stability of the vertical strains. Because of the lack of reliable experimental data, a realistic value of 0.3 is considered a suitable value for the simulations since it provides accurate and stable enough results. The same value has been previously considered in previous simulations [17,54].

5.3. Fracture energy

Fig. 11 shows that the considered range for the fracture energy provides a reasonable approach to the experimental results. Thus, the numerical simulations confirm that the real value of fracture energy of the material might lie within the proposed range. From the different values considered, a fracture energy of 0.008N/mm is considered to provide the most stable and accurate results.

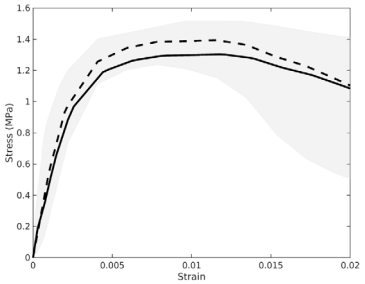

Fig. 14. Stress–strain relationship of the compression test for the optimum model parameters (solid line). The shaded area and the dashed line represent the envelope and the average of the experimental results, respectively.

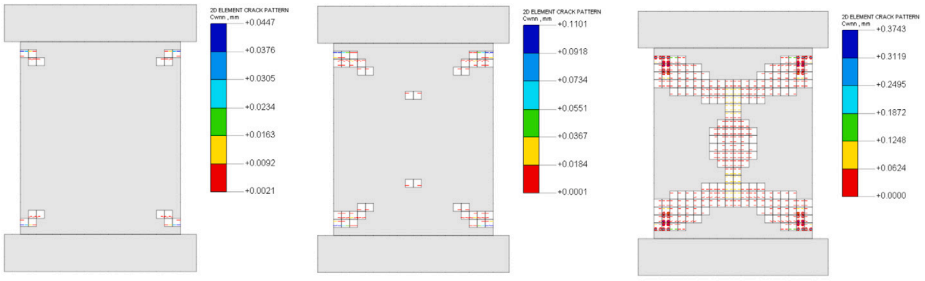

(a) (b) (c)

Fig. 15. Illustration of failure progress from simulations of compression test.

Table 3
Calibrated material properties for adobe masonry.

Elastic			Tension		Compression
E (MPa)	ν	h (mm)	f_t (MPa)	G_f^I (N/mm)	ϵ_p (mm/mm)
642	0.3	25	0.13	0.008	0.002

5.4. Tensile strength

Fig. 12 shows that the experimental estimation of the tensile strength based on the elastic solution of the diagonal compression test problem (0.13 MPa) provides the best fit of the numerical solution with the experimental results. The strength obtained from splitting tests and assuming a pure shear stress state in the diagonal compression test (0.17 MPa), leads to an overestimation of the maximum loading capacity of the wall and higher instabilities. It can be also observed that the tensile strength has a high influence on the limit of the elastic range.

5.5. Element size (mesh refinement)

A parametric analysis to see the minimum element size dimension required for obtaining accurate enough results was also performed. The idea was to find a trade-off between computational time cost and results accuracy. As it is shown in Fig. 13, accurate results are observed for a 25 mm element size. No significant variation is observed in the results when the mesh is refined from 35 mm to 25 mm element size. In contrast, results for a 50 mm element size illustrate that a mesh of that size provides less accurate results, specially for the nonlinear range.

6. Numerical vs experimental results

This section is aimed at providing an assessment of the accuracy of the numerical results obtained with the calibrated parameters selected from the previous sensitivity summarized in Table 3.

First, the results from the simple compression tests are shown in Fig. 14, where a good agreement between the experimental and numerical results is shown. The modulus of elasticity controls the elastic behavior up to the point where cracking starts. Then, when the material cracks, the masonry loses strength capacity due to stiffness degradation. Because of the different parameters involved in the non-linear behavior and failure of the material, the numerical results do not perfectly match the average experimental results; however, the numerical curve fits reasonably the experimental range values.

Fig. 15 illustrates the failure pattern of the walls obtained from the numerical simulations. Although only compression loads are applied on the wall, the failure starts by exceeding the material tensile strength. Then, a progressive diagonal cracking process takes place from the corners of the wall to its center, where a vertical cracked region is formed. This result agrees with the damage pattern observed in the experimental tests (Fig. 3 b), where the cracks also started at the top and bottom sides and formed an X-shape crack pattern. This failure pattern is typical for masonry prisms subjected to axial compression loading. Fig. 15 also shows different stages of the failure process, including numerical values of crack openings (in mm).

For the diagonal compression tests, strains of the numerical model are obtained from the relative displacements between nodes located at the same positions where the displacement sensors were fixed to the wall. Fig. 16 compares the vertical and horizontal strains during the diagonal compression tests. The capital letters in the plot are related to the stress, strain and crack pattern shown in Figs. 17–20. The agreement between the numerical and experimental results is fairly good. The most significant deviation comes from the rapid decrease of the supported load in the numerical simulation just after the maximum load is reached. This phenomenon is due to the softening of the wall's central part when its ultimate strength is reached. This softening procedure is followed by a transition to another load transmission path, in which adjacent areas to the central part (that are not damaged yet and present higher stiffness with a remanent strength reserve) start to support a higher portion of the applied load. This transition is illustrated in Fig. 17. It shows how vertical stresses are redistributed after the peak force is reached. Once the redistribution has taken place, stiffness is recovered, although it progressively decreases, and a final softening behavior is observed when the whole area between the two contact surfaces is cracked. Although a smaller strength reduction due to softening is observed in the numerical results, the obtained numerical stress–strain curves are still within the interval of the experimental results range. This wide range of experimental results actually demonstrates the quasi-brittle behavior of adobe masonry. The strength reduction is directly related to the tensile fracture energy, being the proposed values suitable for obtaining a good agreement with the experimental results in terms of stresses and strains. Fig. 18 illustrates the distribution of horizontal stresses during the test. It can be seen how the central part of the wall reaches first the tensile strength. The evolution of the horizontal strains and crack pattern (Figs. 19 and 20) also illustrate well the failure mechanism. They agree with the experimental failure pattern (Fig. 4(c)), where vertical cracks appeared from top to bottom, inducing the division of the masonry specimens into two big parts.

The comparison between the force vs strain experimental and numerical curves and the cracking process shows that the numerical calibrated total-strain crack model can reproduce well the experimental results. Despite the significant scattering in the experimental results (see Figs. 14 and 16), the numerical results show that practical numerical predictions of the structural response of this kind of adobe walls built in Sevilla can be obtained using the proposed model. Furthermore, among all material properties considered, the tensile strength and the tensile fracture energy are the most parameters(see Figs. 11 and 12), being the tensile fracture energy the one that controls mainly the inelastic response. This preliminary study concludes that even though adobe is a brittle material, it retains some tension fracture energy which controls the crack formation process.

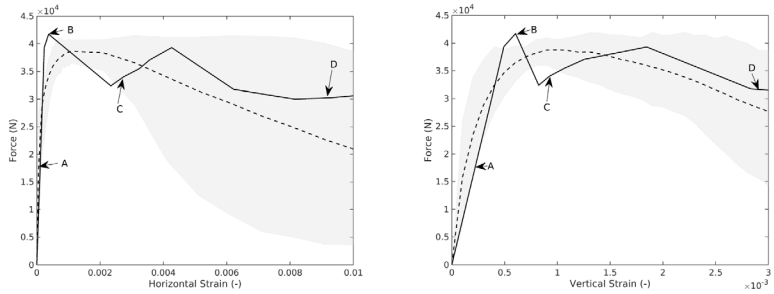

Fig. 16. Relationship between applied force and (a) horizontal strains and (b) vertical strains in the diagonal compression test for the optimum set of model parameters (solid line). The shaded area and the dashed line represent the envelope and the average of the experimental results, respectively.

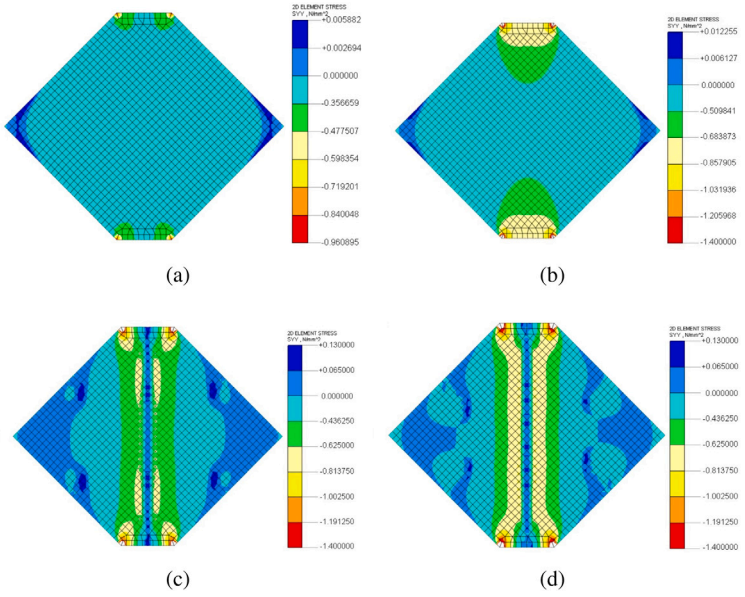

Fig. 17. Representation of vertical stress fields at reference states A, B, C, D (figures (a)–(d), respectively) marked in Fig. 16.

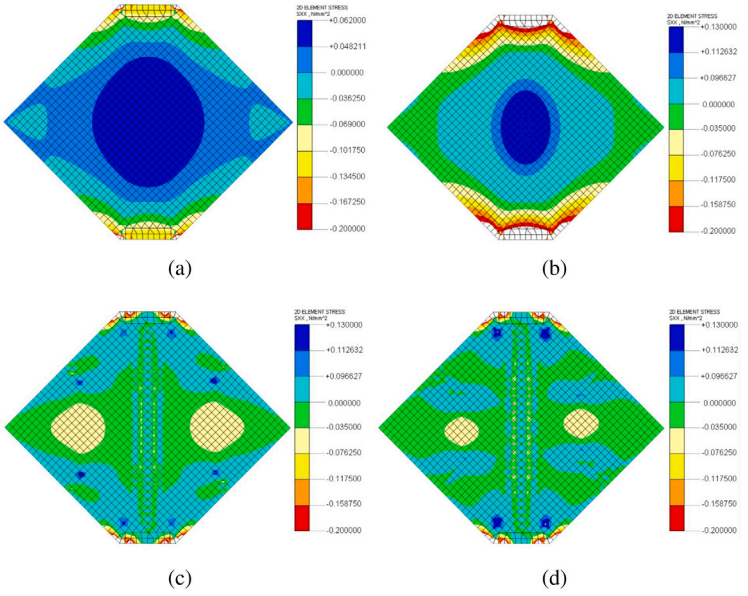

Fig. 18. Representation of horizontal stress fields at reference states A, B, C, D (figures (a)–(d), respectively) marked in Fig. 16.

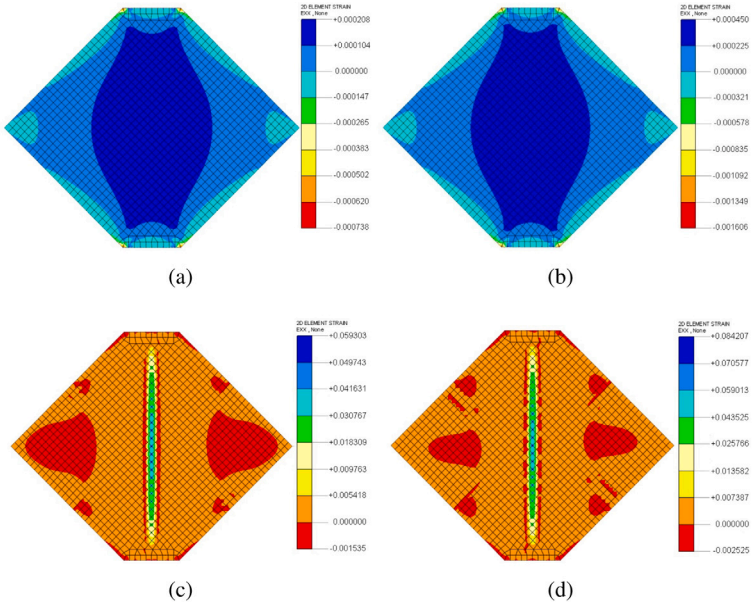

Fig. 19. Representation of horizontal strain fields at reference states A, B, C, D (figures (a)–(d), respectively) marked in Fig. 16.

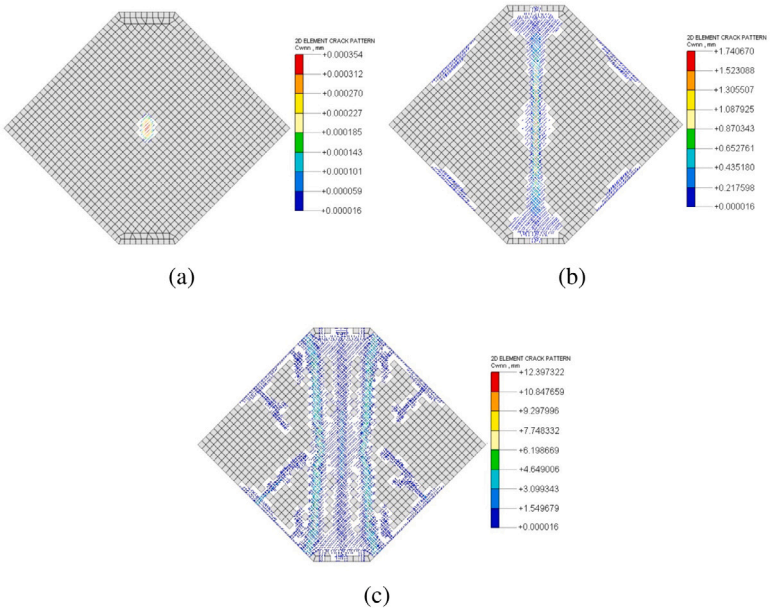

Fig. 20. Crack pattern at reference states B, C, D (figures (a)–(c), respectively)marked in Fig. 16.

Then, since masonry fails due to its low capacity to withstand tensile stresses, any intervention of exiting adobe constructions or proposal for the enhancement of the structural behavior of adobe masonry walls, should be focused on the improvement of its ductility.

7. Conclusions

The experimental behavior of adobe masonry walls in compression and diagonal compression is well represented by a macromechanical approach based on the total strain crack model. The presented results show that accurate simulations of adobe walls can be performed for practical applications using this approach, specially when dealing with large size structures for which the micro-modeling approach is not feasible because of the computational cost.

The constitutive model must be built from reference experimental values. In the present study, a valid model has been built from the experimental compressive constitutive law and experimental tensile strength. Some parameters are estimated from the literature, although special attention should be paid to fracture energy and tensile strength, which are the most influential parameters on the final results. Other parameters such as Poisson modulus do not significantly affect the results and uncertainty about its real value is not a major issue.

Regarding the tensile strength, the presented results show that a realistic value based on experimental tests is required. The estimation of the tensile strength based on the linear elastic solution from the diagonal compression tests should be considered rather than the pure shear stress state assumption or the use of splitting tests.

Fracture energy is a very important parameter for which few experimental information exists in the literature. The sensitivity analysis presented in this paper suggests a value of 0.008 N/mm for modeling adobe walls. Moreover, the experimental procedure to estimate its value is not clearly established yet. Thus, further research is required

in order to establish a valid procedure that should be also validated by its use on numerical models.

Additionally, further research should also be dedicated to the investigation of non isotropy laws to reproduce, within the macro modeling approach, the failure process of adobe masonry.

The present paper shows that the followed methodology for the calibration of the mechanical parameters of adobe masonry is a suitable approach for the numerical modeling of this material.

CRediT authorship contribution statement

J.M. Fages: Software, Formal analysis, Methodology, Investigation. **N. Tarque:** Term, Software, Conceptualization, Methodology. **J.D. Rodríguez-Mariscal:** Investigation, Resources, Writing – original draft, Writing – review & editing. **M. Solís:** Term, Conceptualization, Supervision, Writing – original draft, Writing – review & editing, Supervision.

Declaration of competing interest

The authors declare that they have no known competing financial interests or personal relationships that could have appeared to influence the work reported in this paper.

Data availability

Data will be made available on request.

Acknowledgments

This work was supported by the Spanish Ministry of Science, Spain, Innovation and Universities (Ministerio de Ciencia, Innovación *y* Universidades), Spain through research project PID2019-109622RB-C21.

References

[1] N. Tarque, M. Blondet, J. Vargas Neumann, Rope mesh as a seismic reinforcement for two-storey adobe buildings, Bull. Earthq. Eng. (2022) http://dx.doi.org/10.1007/s10518-022-01346-7.

[2] J. Cid, F.R. Mazarrón, I. Cañas, I. Cañas, Las normativas de construcción con tierra en el mundo, Inf. Constr. 63 (523) (2011) 159–169, http://dx.doi.org/10.3989/ic.10.011, URL http://informesdelaconstruccion.revistas.csic.es/index.php/informesdelaconstruccion/article/view/1262/1347.

[3] H. Schroeder, Modern earth building codes, standards and normative development, in: M.R. Hall, R. Lindsay, M. Krayenhoff (Eds.), Modern Earth Buildings, in: Woodhead Publishing Series in Energy, Woodhead Publishing, 2012, pp. 72–109, http://dx.doi.org/10.1533/9780857096166.1.72, URL https://www.sciencedirect.com/science/article/pii/B9780857090263500046.

[4] Y. Hurol, H. Yüceer, Ö. Sahali, Building code challenging the ethics behind adobe architecture in north cyprus, Sci. Eng. Ethics 21 (2015) 381–399, http://dx.doi.org/10.1007/s11948-014-9533-0.

[5] M. Correia, Conservation in Earthen Heritage — Assessment and Significance of Failure, Criteria, Conservation Theory, and Strategies, Cambridge Scholar Publishing, Newcastle, UK, 2016.

[6] T.L. Piani, D. Krabbenborg, J. Weerheijm, L. Koene, L.J. Sluijs, The mechanical performance of traditional adobe masonry components: an experimental-analytical characterization of soil bricks and mud mortar, J. Green Build. 13 (3) (2018) 17–44, http://dx.doi.org/10.3992/1943-4618.13.3.17.

[7] F. Pacheco-Torgal, S. Jalali, Earth construction: Lessons from the past for future eco-efficient construction, Constr. Build. Mater. 29 (Supplement C) (2012) 512–519, http://dx.doi.org/10.1016/j.conbuildmat.2011.10.054, URL http://www.sciencedirect.com/science/article/pii/S0950061811006039.

[8] H. Niroumand, J.A. Barceló Álvarez, M. Saaly, Investigation of earth building and earth architecture according to interest and involvement levels in various countries, Renew. Sustain. Energy Rev. 57 (2016) 1390–1397, http://dx.doi.org/10.1016/j.rser.2015.12.183, URL https://www.sciencedirect.com/science/article/pii/S136403211501566X.

[9] A. Eslami, H.R. Ronagh, S.S. Mahini, R. Morshed, Experimental investigation and nonlinear FE analysis of historical masonry buildings - A case study, Constr. Build. Mater. 35 (2012) 251–260, http://dx.doi.org/10.1016/j.conbuildmat.2012.04.002.

[10] R. Illampas, D.C. Charmpis, I. Ioannou, Laboratory testing and finite element simulation of the structural response of an adobe masonry building under horizontal loading, Eng. Struct. 80 (2014) 362–376, http://dx.doi.org/10.1016/j.engstruct.2014.09.008, URL http://www.sciencedirect.com/science/article/pii/S0141029614005446.

[11] M.C. Jiménez Delgado, I. Cañas Guerrero, Earth building in Spain, Constr. Build. Mater. 20 (9) (2006) 679–690, http://dx.doi.org/10.1016/j.conbuildmat.2005.02.006", URL http://www.sciencedirect.com/science/article/B6V2G-4G0M3N7-1/2/d4a12a3c29a9c967a5d7d74e6d2941bf.

[12] C. Mileto, F.V. López-Manzanares, L. García-Soriano, V. Cristini (Eds.), Vernacular Earthen Architecture, Conservation and Sustainability (SosTierra 2017, Valencia, Spain, 14-16 September 2017), CRC Press, 2017.

[13] C. Mileto, F. Vegas López-Manzanares, L. Villacampa Crespo, L. García-Soriano, The influence of geographical factors in traditional earthen architecture: The case of the Iberian Peninsula, Sustainability 11 (8) (2019) 2369, http://dx.doi.org/10.3390/su11082369, URL https://www.mdpi.com/2071-1050/11/8/2369.

[14] C. Oliveira, D. Silveira, H. Varum, F. Parisi, L. Miccoli, M. Solís, J.D. Rodríguez-Mariscal, N. Tarque, Mechanical characterization of adobe masonry, in: H. Varum, F. Parisi, N. Tarque, D. Silveira (Eds.), Structural Characterization and Seismic Retrofitting of Adobe Constructions: Experimental and Numerical Developments, Springer International Publishing, Cham, Switzerland, 2021, pp. 55–93, http://dx.doi.org/10.1007/978-3-030-74737-4-4.

[15] D. Silveira, C. Oliveira, H. Varum, I. Ioannou, L. Miccoli, Tarque Nicola, Parisi Fulvio, L. Fenu, M. Solís, J.D. Rodríguez-Mariscal, Mechanical characterization of adobe bricks, in: H. Varum, F. Parisi, N. Tarque, D. Silveira (Eds.), Structural Characterization and Seismic Retrofitting of Adobe Constructions: Experimental and Numerical Developments, Springer International Publishing, Cham, Switzerland, 2021, pp. 55–93, http://dx.doi.org/10.1007/978-3-030-74737-4-4.

[16] N. Tarque, G. Camata, H. Varum, E. Spacone, M. Blondet, Numerical simulation of an adobe wall under in-plane loading, Earthq. Struct. 6 (6) (2014) 627–646, http://dx.doi.org/10.12989/eas.2014.6.6.627.

[17] L. Miccoli, A. Garofano, P. Fontana, U. Müller, Experimental testing and finite element modelling of earth block masonry, Eng. Struct. 104 (2015) 80–94, http://dx.doi.org/10.1016/j.engstruct.2015.09.020, URL http://linkinghub.elsevier.com/retrieve/pii/S014102961500591X.

[18] S.H. Rafsanjani, A. Bakhshi, M.A. Ghannad, M. Yekrangnia, F. Soumi, Predictive Tri-Linear Benchmark Curve for In-Plane Behavior of Adobe Walls. Vol. 9, (8) Taylor & Francis, 2015, pp. 986–1004, http://dx.doi.org/10.1080/15583058.2014.899408, URL https://www.tandfonline.com/doi/abs/10.1080/15583058.2014.899408.

[19] F. Parisi, C. Balestrieri, H. Varum, Nonlinear finite element model for traditional adobe masonry, Constr. Build. Mater. 223 (2019) 450–462, http://dx.doi.org/10.1016/j.conbuildmat.2019.07.001, URL https://linkinghub.elsevier.com/retrieve/pii/S0950061819316642.

[20] J.D. Rodríguez-Mariscal, Q. Ma, M. Solís, Experimental analysis of diagonal compression and splitting tests for the characterization of shear and tensile behavior of adobe masonry, Eng. Struct. 215 (2020) 110633, http://dx.doi.org/10.1016/j.engstruct.2020.110633.

[21] F. Parisi, D. Daudon, R. Illampas, P. Lourenço, N. Tarque, Numerical modelling of adobe structures, in: H. Varum, F. Parisi, N. Tarque, D. Silveira (Eds.), Structural Characterization and Seismic Retrofitting of Adobe Constructions: Experimental and Numerical Developments, Springer International Publishing, Cham, Switzerland, 2021, pp. 55–93, http://dx.doi.org/10.1007/978-3-030-74737-4-4.

[22] J. Lubliner, J. Oliver, S. Oller, E. Oñate, A plastic-damage model for concrete, Int. J. Solids Struct. 25 (3) (1989) 299–326, http://dx.doi.org/10.1016/0020-7683(89)90050-4.

[23] P. Lourenço, Computational Strategy for Masonry Structures (Ph.D. thesis), Delft University of Technology, 1996.

[24] J. Rodríguez-Mariscal, M. Solís, Hacia una metodología para la caracterización experimental del comportamiento a compresión de la mampostería de adobe, Inf. Constr. 72 (557) (2020) e332, http://dx.doi.org/10.3989/ic.67456.

[25] ASTM, Standard test method for diagonal tension (Shear) in masonry assemblages BT - standard test method for diagonal tension (shear) in masonry assemblages, 1988.

[26] RILEM TC, Diagonal tensile strength tests of small wall specimens, in: RILEM Recommendations for the Testing and Use of Constructions Materials, E & FN SPON, 1994, pp. 488–489.

[27] D. Silveira, H. Varum, A. Costa, J. Carvalho, Mechanical properties and behavior of traditional adobe wall panels of the aveiro district, J. Mater. Civ. Eng. 27 (9) (2015) 04014253, http://dx.doi.org/10.1061/(ASCE)MT.1943-5533.0001194, URL http://ascelibrary.org/doi/10.1061/%28ASCE%29MT.1943-5533.0001194.

[28] L. Miccoli, D.V. Oliveira, R.A. Silva, U. Müller, L. Schueremans, Static behaviour of rammed earth: experimental testing and finite element modelling, Mater. Struct. 48 (10) (2015) 3443–3456, http://dx.doi.org/10.1617/s11527-014-0411-7.

[29] F. Wu, G. Li, H.-N. Li, J.-Q. Jia, Strength and stress–strain characteristics of traditional adobe block and masonry, Mater. Struct. 46 (9) (2013) 1449–1457, http://dx.doi.org/10.1617/s11527-012-9987-y, URL http://link.springer.com/10.1617/s11527-012-9987-y.

[30] R. Illampas, I. Ioannou, D.C. Charmpis, Experimental assessment of adobe masonry assemblages under monotonic and loading-unloading compression, Mater. Struct. 50 (79) (2017) http://dx.doi.org/10.1617/s11527-016-0952-z.

[31] P. Müller, L. Miccoli, P. Fontana, C. Ziegert, Development of partial safety factors for earth block masonry, Mater. Struct. 50 (31) (2016) 31, http://dx.doi.org/10.1617/s11527-016-0902-9.

[32] A. Shabani, M. Kioumarsi, A novel macroelement for seismic analysis of unreinforced masonry buildings based on MVLEM in OpenSees, J. Build. Eng. 49 (2022) 104019, http://dx.doi.org/10.1016/j.jobe.2022.104019, URL https://www.sciencedirect.com/science/article/pii/S2352710222000328.

[33] J. Rots, Numerical simulation of cracking in structural masonry, Heron 36 (2) (1991) 47–52.

[34] P. Roca, M. Cervera, G. Gariup, L. Pela', P. Roca, M. Cervera, G. Gariup, M. Cervera, G. Gariup, L. Pela', Structural analysis of masonry historical constructions. Classical and advanced approaches, Arch. Comput. Methods Eng. 17 (3) (2010) 299–325, http://dx.doi.org/10.1007/S11831-010-9046-1, URL https://link.springer.com/article/10.1007/s11831-010-9046-1.

[35] C. Sui, M.Y. Rafiq, Laterally loaded masonry wall panels: a review of numerical models, J. Int. Mason. Soc. 22 (2) (2009) 47–53.

[36] A. Cecchi, M. G., T. A., Validation of analytical multiparameter homogenization models for out-of-plane loaded masonry walls by means of the finite element method, J. Eng. Mech. 131 (2) (2005) 185–198, http://dx.doi.org/10.1061/(ASCE)0733-9399(2005)131:2(185), arXiv:https://ascelibrary.org/doi/pdf/10.1061/%28ASCE%290733-9399%282005%29131%3A2%28185%29, URL https://ascelibrary.org/doi/abs/10.1061/%28ASCE%290733-9399%282005%29131%3A2%28185%29.

[37] G. Milani, P.B. Lourenço, A. Tralli, Homogenized rigid-plastic model for masonry walls subjected to impact, Int. J. Solids Struct. 46 (22) (2009) 4133–4149, http://dx.doi.org/10.1016/j.ijsolstr.2009.08.007, URL https://www.sciencedirect.com/science/article/pii/S0020768309003060.

[38] G. Milani, P. Lourenço, A. Tralli, Homogenised limit analysis of masonry walls, Part I: Failure surfaces, Comput. Struct. 84 (3) (2006) 166–180, http://dx.doi.org/10.1016/j.compstruc.2005.09.005, URL https://www.sciencedirect.com/science/article/pii/S0045794905003159.

[39] A. Zucchini, P. Lourenço, A micro-mechanical homogenisation model for masonry: Application to shear walls, Int. J. Solids Struct. 46 (3) (2009) 871–886, http://dx.doi.org/10.1016/j.ijsolstr.2008.09.034, URL https://www.sciencedirect.com/science/article/pii/S0020768308004174.

[40] L. Pelà, M. Cervera, P. Roca, An orthotropic damage model for the analysis of masonry structures, Constr. Build. Mater. 41 (2013) 957–967, http://dx.doi.org/10.1016/j.conbuildmat.2012.07.014, URL https://www.sciencedirect.com/science/article/pii/S0950061812004837.

[41] F.J. Vecchio, M.P. Collins, Compression response of cracked reinforced concrete, J. Struct. Eng. 119 (12) (1993) 3590–3610, http://dx.doi.org/10.1061/(ASCE)0733-9445(1993)119:12(3590), arXiv:https://ascelibrary.org/doi/pdf/10.1061/%28ASCE%290733-9445%281993%29119%3A12%283590%29, URL https://ascelibrary.org/doi/abs/10.1061/%28ASCE%290733-9445%281993%29119%3A12%283590%29.

[42] R.G. Selby, F.J. Vecchio, Three-Dimensional Constitutive Relations for Reinforced Concrete, University of Toronto, Dept. of Civil Engineering, [Toronto], 1993.

[43] G. Schreppers, A. Garofano, F. Messali, J. Rots, DIANA Validation Report for Masonry Modelling, DIANA FEA Report 2016-DIANA-R1601; TU Delft Structural Mechanics CiTG Report CM-2016-17, 2017, pp. 1–143.

[44] M. Sousamli, F. Messali, J.G. Rots, A total-strain based orthotropic continuum model for the cyclic nonlinear behavior of unreinforced brick masonry structures, Internat. J. Numer. Methods Engrg. 123 (8) (2022) 1813–1840, http://dx.doi.org/10.1002/nme.6917, arXiv:https://onlinelibrary.wiley.com/doi/pdf/10.1002/nme.6917, URL https://onlinelibrary.wiley.com/doi/abs/10.1002/nme.6917.

[45] P.H. Feenstra, J.G. Rots, Comparison of concrete models for cyclic loading, in: P. Benson Shing, T. Tanabe (Eds.), Modelling of Inelastic Behaviour of RC Structures under Seismis Loads, American Society of Civil Engineers, 2001, pp. 38–55.

[46] F.J. Vecchio, M.P. Collins, The modified compression field theory for reinforced concrete elements subjected to shear, ACI J. 22 (1986) 219–231.

[47] P.B. Lourenço, Experimental and numerical issues in the modelling of the mechanical behaviour of masonry, in: P. Roca, J. González, E. Oñate, P. Lourenço (Eds.), Proceedings of Structural Analysis of Historical Constructions II, CIMNE, Barcelona, spain, 1998.

[48] M. Jirasek, Objective modeling of strain localization, Rev. Fr. Génie Civ. 6 (6) (2002) 1119–1132, http://dx.doi.org/10.1080/12795119.2002.9692735.

[49] M. Jirasek, M. Bauer, Numerical aspects of the crack band approach, Comput. Struct. 110–111 (2012) 60–78, http://dx.doi.org/10.1016/j.compstruc.2012.06.006, URL https://www.sciencedirect.com/science/article/pii/S0045794912001575.

[50] B. Lopes, M. Arruda, L. Almeida-Fernandes, L. Castro, N. Silvestre, J. Correia, Assessment of mesh dependency in the numerical simulation of compact tension tests for orthotropic materials, Compos. C Open Access 1 (2020) 100006, http://dx.doi.org/10.1016/j.jcomc.2020.100006, URL https://www.sciencedirect.com/science/article/pii/S2666682020300062.

[51] A. Earij, G. Alfano, K. Cashell, X. Zhou, Nonlinear three–dimensional finite–element modelling of reinforced–concrete beams: Computational challenges and experimental validation, Eng. Fail. Anal. 82 (2017) 92–115, http://dx.doi.org/10.1016/j.engfailanal.2017.08.025, URL https://www.sciencedirect.com/science/article/pii/S1350630717303151.

[52] J.A.P.P. Almeida, Mechanical Characterization of Traditional Adobe Masonry Elements (Ph.D. thesis), 2012, p. 75, URL https://www.proquest.com/dissertations-theses/mechanical-characterization-traditional-adobe/docview/2586971474/se-2?accountid=14744.

[53] K.F. Abdulla, L.S. Cunningham, M. Gillie, Experimental study on the mechanical properties of straw fiber–reinforced adobe masonry, J. Mater. Civ. Eng. 32 (11) (2020) 4020322, http://dx.doi.org/10.1061/(ASCE)MT.1943-5533.0003410, URL https://www.research.manchester.ac.uk/portal/files/175768576/Abdulla_et_al_ASCE_J_of_Materials_in_Civil_Eng_Author_Accepted_Jul2020.pdf.

[54] A. Caporale, F. Parisi, D. Asprone, R. Luciano, A. Prota, Critical surfaces for adobe masonry: Micromechanical approach, Composites B 56 (2014) 790–796, http://dx.doi.org/10.1016/j.compositesb.2013.08.087, URL https://linkinghub.elsevier.com/retrieve/pii/S135983681300509X.